

# We are IntechOpen, the world's leading publisher of Open Access books Built by scientists, for scientists

## 4,800

Open access books available

## 122,000

International authors and editors

## 135M

Downloads

Our authors are among the

## 154

Countries delivered to

## TOP 1%

most cited scientists

## 12.2%

Contributors from top 500 universities

**WEB OF SCIENCE™**Selection of our books indexed in the Book Citation Index  
in Web of Science™ Core Collection (BKCI)

Interested in publishing with us?  
Contact [book.department@intechopen.com](mailto:book.department@intechopen.com)

Numbers displayed above are based on latest data collected.

For more information visit [www.intechopen.com](http://www.intechopen.com)

# Block Diagram Programming of Quantum Dot Sources and Infrared Photodetectors for Gamma Radiation Detection Through VisSim

Mohamed S. El-Tokhy<sup>1</sup>, Imbaby I. Mahmoud<sup>1</sup>, and Hussein A. Konber<sup>2</sup>

<sup>1</sup>Engineering Department, NRC, Atomic Energy Authority, Inshas, Cairo

<sup>2</sup>Electrical Engineering Department, Al Azhar University, Nasr City, Cairo  
Egypt

## 1. Introduction

Quantum dots (QDs) have attracted tremendous interest over the last few years for a large variety of applications ranging from optoelectronic through photocatalytic to biomedical, including applications as nanophosphors in light emitting diodes LEDs [1]. QDs have been suggested as scintillators for detection of alpha particles and gamma-rays [1-4]. Quantum dots offer an improvement on scintillator technology in that the size of the phosphorescent material would not be restrained by crystal growth. The dots would be suspended in a transparent matrix that could be as large as desired. Moreover, the output of the QDs is a function of their dimensions. Therefore, they could be produced to emit light at wavelengths suitable for detection by avalanche photodiodes. That offer higher quantum efficiencies than photomultiplier tubes. Therefore, the sensitivity of the scintillator detector is increased [5]. To our knowledge, still models describing QD sources as gamma detection are not devised yet. In this chapter, we report on the effects of gamma irradiation on the different properties of CdSe/ZnS QDs. These characteristics are optical gain, power, population inversion and photon density. Furthermore, a new semiconductor scintillator detector was studied in which high-energy gamma radiation produces electron-hole pairs in a direct-gap semiconductor material that subsequently undergo interband recombination, producing infrared light to be registered by a photo-detector [6]. Therefore, quantum dot infrared photodetectors (QDIPs) can be used for this purpose. This chapter presents a method to evaluate, study, and improve the performance of quantum dot sources and infrared photodetectors as gamma radiation detection. This chapter is organized as follows: Section 3.2 presents the basics of VisSim simulator. QD devices as a detector are illustrated in Section 3.3. The proposed models of both quantum dot devices are represented in Section 3.4. Discussion and results are summarized in Section 3.5.

## 1.2 VisSim simulator

VisSim simulation is one of the most widely used environments in operations research and management science, and by all indications its popularity is on the increase. The goal of using VisSim modeling and analysis is to give an up-to-date treatment of all the important aspects of a simulation study, including modeling, simulation languages, validation, and output data

analysis. However, most real world-systems are too complex to allow realistic models to be evaluated analytically, and these models must be studied by means of VisSim simulation. In VisSim we use a computer to evaluate a model numerically over a time period of interest, and data are gathered to estimate the desired true characteristics of the model. In addition we have tried to represent the operation of the QD sources and photodetectors in a manner understandable to a person having only a basic familiarity with its main behaviors such as optical gain, power, output photon densities, dark current, photocurrent, and detectivity. It can be a powerful supplement to traditional design techniques.

System engineering program such as Mathsoft's VisSim employ the Graphical User Interface (GUI) concept. In order to, display systems of differential equations as feedback systems. Additionally, if the relationships which compose the model are simple enough, it may be possible to use VisSim simulation model. Then, assume numerical integration using the methods of Laplace transforms for differential equations, hence the appearance of the symbols  $1/S$ , to indicate integration. Though these packages integration is used because it is an inherently more stable numerical operation. The first step in converting from equation to block diagram form is thus to integrate both sides of differential equation. The operations of addition, multiplication, integration and so on are performed by blocks operators, as shown in the following models. Besides, reading the block diagram is from left to right.

The following are some possible reasons for the widespread popularity of the VisSim simulation [7-10]:

1. Most complex, real-world systems with stochastic elements cannot be accurately described by a mathematical model which can be evaluated analytically. Thus, VisSim simulation is often the main type of investigation possible.
2. VisSim Simulation allows one to estimate the performance of an exciting system under some projected set of operation conditions.
3. Alternative proposed system designs (or alternative operating policies for a single system) can be compared via VisSim simulation to see which best meets specified requirements.
4. In VisSim simulation we can maintain much better control over experimental conditions than would generally be possible when experimenting with the system itself.
5. VisSim Simulation allows us to study a system with along time frame, or alternatively to study the detailed workings of a system in expanded time.

Our goal in this chapter is to evaluate the performance of QDs devices by using VisSim environment along with the block diagram programming procedures.

### 1.3 QD devices as a detector

Quantum dots have been used in a wide variety of applications. A key advantage of these particles is that their optical properties depend predictably on size, which enables tuning of the emission wavelength [11]. QD devices as a source and infrared photodetectors can be used to detect gamma radiation [2, 4, 6]. Moreover, the ability of semiconductor quantum dots to convert alpha radiation into visible photons was demonstrated in [2].

In this chapter, we report on the scintillation of quantum dots sources and infrared photodetectors under gamma-ray irradiation.

Semiconductor scintillation gamma radiation detector based on QD will be discussed in which the gamma-ray absorbing semiconductor body is impregnated with multiple small

direct gap semiconductor inclusions of band gap slightly narrower than that of the body. If the typical distance between them is smaller than the diffusion length of carriers in the body material, the photo-generated electrons and holes will recombine inside the impregnations and produce scintillating radiation to which the wide gap body is essentially transparent [6]. Furthermore, the quantum dot lasers (QDLs) under gamma radiation is characterized by changes in threshold current, external slope efficiency and light output [12].

For infrared (IR) detection, most of QDIPs are based on vertical heterostructures consisting of two dimensional arrays of QDs separated by the barrier layers. The QD structures serving as the photodetector active region, where IR radiation is absorbed, are sandwiched between heavily doped emitter and collector contact layers. The active region can be either doped (with dopants of the same type as the contact layers) or undoped. Schematic view of vertical QDIPs device structures is in [13]. The absorption of IR is associated with the electron intersubband transitions from bound states in QDs into continuum states above the barriers or into excited quasi-bound states near the barrier top. The bound-to-continuum transitions or bound-to-quasi-bound transitions followed by fast escape into the continuum result in the photoionization of QDs and the appearance of mobile electrons. Bound electrons accumulated in QDs can create a significant space charge in the active region. In this chapter, we extended the same physical characteristics to study QD devices under gamma radiation.

## 1.4 The proposed models of quantum dot devices

### 1.4.1 The proposed simulator of quantum dot laser under gamma radiation

Improved radiation detection using quantum dot semiconductor composites is demonstrated [4, 14]. The quantum confinement effects enabled the QDs to be used with a wide variety of detectors. The inorganic nanocrystalline quantum dots will be demonstrated as a powerful method in preparing scintillating devices. In gamma-ray detection, our first goal is to employ nanomaterials in the form of QD based mixed matrices to achieve scintillation output several times over that from NaI(Tl) crystals. Moreover, block diagram models are used to represent carrier densities in the Subbands, population inversion process, optical power, and gain. Our goal from this study is to obtain a device that has high performance with optimal operating conditions.

#### 1.4.1.1 Proposed simulator of optical wavelength

This subsection introduces a useful block diagram model to predict effect of incident gamma radiation on quantum dot emission wavelength.

The QDs semiconductor composite is designed so that ionizing radiation produces excitations predominantly in the semiconductor QDs. These excitations are subsequently Förster-transferred to organic material. For scintillators, the composite material must be transparent to the emitted photon, and the large Stokes shift of the organic material is essential. For charge-collection devices the composite material must be trap free to allow efficient charge collection. Trap-free, conjugated organic materials are now available [4]. Pure QDs solids are impractical radiation-detection materials because they are not transparent to their emission wavelength and have significant charge-carrier trapping.

If the peak photoluminescence (PL) photon emission energy,  $E_{PL}$ , is always lower than the 1s-1s absorbance peak energy,  $E_{abs}$ , by an energy shift ( $\Delta E_{AP} \sim -0.14 \text{ eV} + 0.074 \times E_{abs}$  or  $\Delta E_{AP} \sim 0.025 \text{ eV}$  for CdSe quantum dots when  $2 \text{ eV} < E_{abs} < 2.5 \text{ eV}$ ), then the wavelength of the PL peak,  $\lambda_{PL}$ , can be calculated as follows [15]

$$\lambda_{PL} = \frac{hc}{E_g + X/R - \Delta E_{AP}} \quad (3.1)$$

where  $h$ ,  $c$ ,  $E_g$ ,  $X$  denote plank's constant, speed of light, energy gap, and  $X = 0.82 \times 10^{-7}$  eV-cm for CdSe, respectively. If all Cd precursors have been consumed, the average nanocrystal radius reaches the completion radius,  $R_c$ , and PL emission occurs at a completion wavelength,  $\lambda_c$ .

$$\lambda_c = \lambda_{PL}|_{R=R_c} \quad (3.2)$$

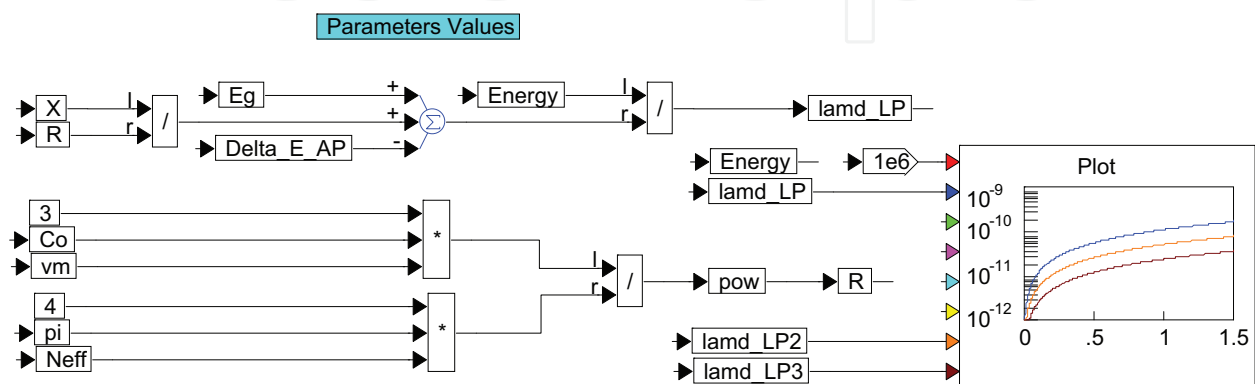


Fig. 3.1. Block diagram model that describes the effect of incident gamma energy on emission wavelength.

Growth of the average quantum dot radius can be written as [15]

$$R_c = \left( \frac{3C_0V_m}{4\pi N_{eff}} \right)^{1/3} \quad (3.3)$$

where  $C_0$ ,  $N_{eff}$ , and  $V_m$  denote the original molar concentration of Cd in the batch (in moles  $\text{cm}^{-3}$ ), the effective number of spherical nanocrystals that would contain the number of moles of Cd that have been consumed, and the molar volume, respectively. Block diagram model that describe the effect of  $\gamma$ -energy on the emission wavelength is depicted in Fig. 3.1.

#### 1.4.2 The models of quantum dot infrared photodetectors

A new scintillation-type semiconductor detector was studied in which high-energy radiation produces electron-hole pairs in a direct-gap semiconductor material that subsequently undergo interband recombination, producing infrared light to be registered by a QDIP. Scintillators are not normally made of semiconductor material. The key issue in implementing a semiconductor scintillator is how to make the material essentially transparent to its own infrared light. Consequently, that photons generated deep inside the semiconductor slab could reach its surface without tangible attenuation.

In this subsection, different treatments are applied to model the characteristics of QDIPs than that in [16-17] under gamma radiation. Furthermore, we will utilize a new block diagram model to consider the characteristics of a QDIP under dark and illumination condition.

### 1.4.2.1 Dark current density block diagram of QDIP

If the numbers of electrons in QDs are sufficiently large, we may assume that these numbers are approximately the same for all QDs in a particular QD array,  $N_k^{i,j} = \langle N_k \rangle$  where  $i$  and  $j$  are the in-plane indices of QDs,  $\langle N_k \rangle$  denotes average extra carrier number in the QDs and  $k$  is the index of the QD array. In this case, the distribution of the electric potential  $\varphi = \varphi(x, y, z)$  in the active region is governed by the Poisson equation [16]

$$\left( \frac{\partial^2}{\partial x^2} + \frac{\partial^2}{\partial y^2} + \frac{\partial^2}{\partial z^2} \right) \varphi = \frac{4\pi q}{\epsilon} \left( \sum_{i,j,k} \langle N \rangle \delta_{11}(x-x_i) \delta_{11}(y-y_j) \delta_{\perp}(z-z_k) - \rho_D \right) \quad (3.4)$$

where  $q$  is the electron charge,  $\epsilon$  is the dielectric constant of the material from which the QD is fabricated,  $\delta_{11}(x)$ ,  $\delta_{11}(y)$ , and  $\delta_{\perp}(z)$  are the QD form-factors in lateral (in the QD array plane) and transverse (growth) directions, respectively,  $x_i$  and  $y_j$  are the in-plane QD coordinates,  $z_k = kL$  is the coordinate of the  $k^{\text{th}}$  QD array (where  $k = 1, 2, 3, \dots, M$  and  $M$  is the number of the QD arrays in the QDIP),  $L$  is the transverse spacing between QDs and  $\rho_D$  is the donor concentration in the active region. The form-factors correspond to the lateral and transverse sizes of QDs equal to  $a_{\text{QD}}$  and  $l_{\text{QD}}$ , respectively.

Moreover, block diagram model that describes the relation between dark current and structural parameters is implemented through VisSim as depicted in Fig. 3.2.

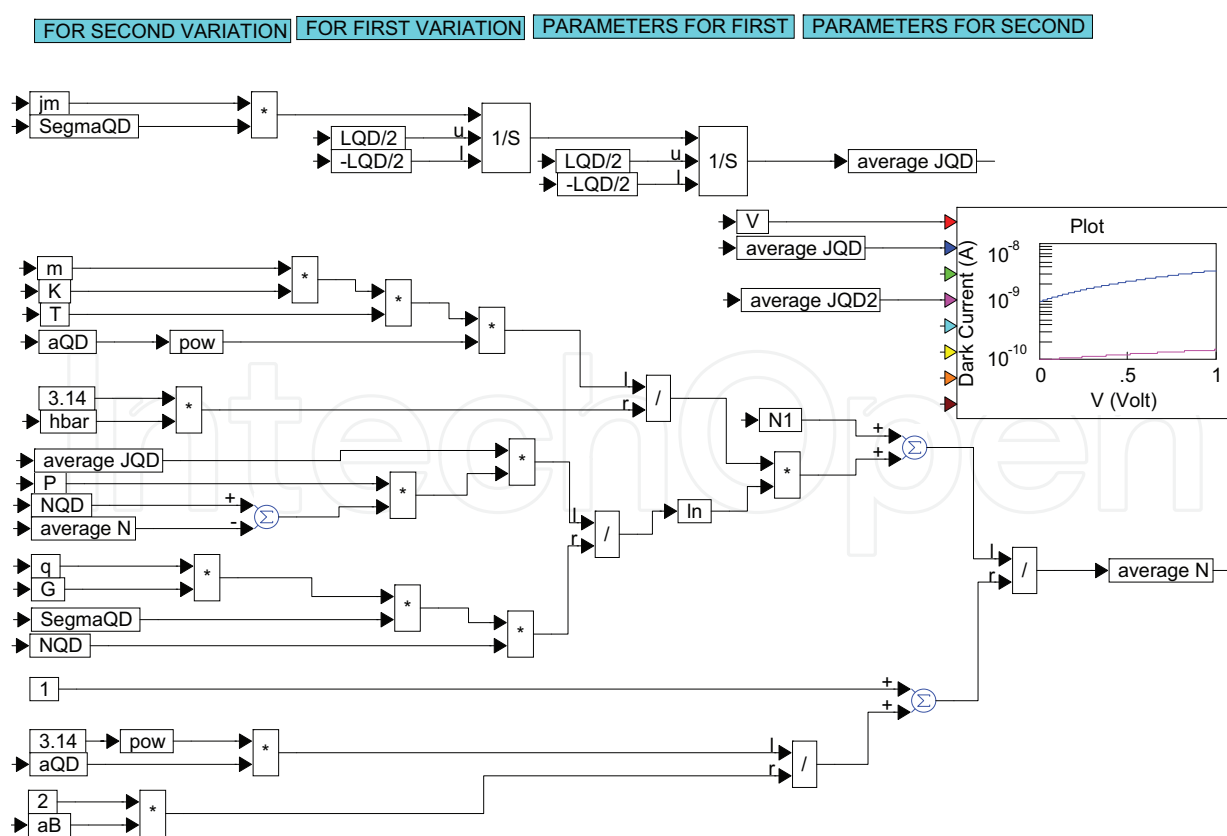


Fig. 3.2. Dark current density block diagram model of QDIPs.

### 1.4.2.2 Photocurrent density block diagram model of QDIP

We calculate the photocurrent density in QDIPs using a developed device model of [16]. This model takes into account the space charge and the self-consistent electric potential in the QDIP active region, the activation character of the electron capture and its limitation by the Pauli principle, the thermionic electron emission from QDs and thermionic injection of electrons from the emitter contact into the QDIP active region, and the existence of the punctures between QDs. The developed model yields the photocurrent density in a QDIP as a function of its structural parameters. The photocurrent density of QDIP is given by [16-17]

$$J_{Photo} = J_m e^{\frac{q\phi}{K_B T}} \quad (3.5)$$

where  $J_m$  is the maximum current density which can be supplied by the emitter contact. The average photocurrent density of QDIP is given by [16-17]

$$\langle J_{Photo} \rangle = \Sigma_{QD} \int_{-\frac{L_{QD}}{2}}^{\frac{L_{QD}}{2}} \int_{-\frac{L_{QD}}{2}}^{\frac{L_{QD}}{2}} J_{Photo} dx dy = J_m \Sigma_{QD} \int_{-\frac{L_{QD}}{2}}^{\frac{L_{QD}}{2}} \int_{-\frac{L_{QD}}{2}}^{\frac{L_{QD}}{2}} e^{\frac{q\phi}{K_B T}} dx dy \quad (3.6)$$

Moreover, block diagram model that describes the relation between photocurrent and structural parameters is implemented through VisSim as shown in Fig. 3.3.

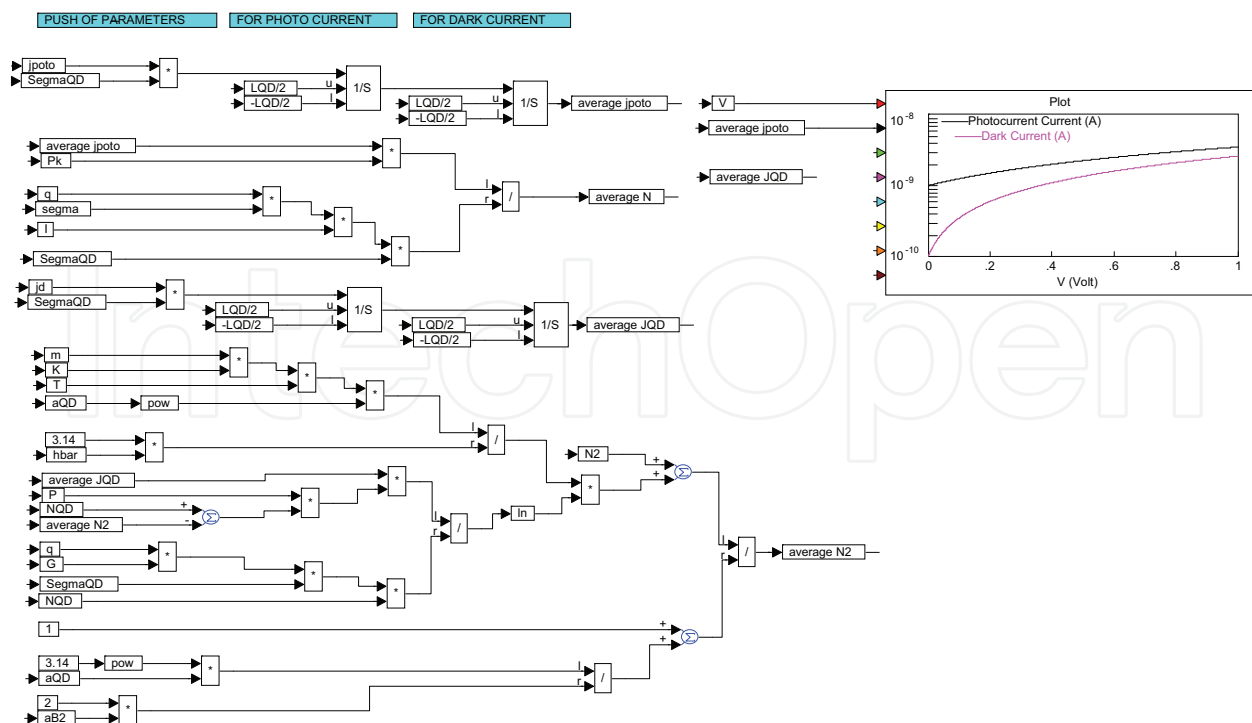


Fig. 3.3. Photocurrent density block diagram model of QDIPs.

### 1.4.2.3 Detectivity block diagram model of QDIP

The specific detectivity,  $D$ , which is a measure of the signal-to-noise ratio of the device, used to characterize QDIPs [18]. It was calculated from the noise density spectra and the peak responsivity [19]. The detectivity of QDIP is determined by the following equation [20-23];

$$D = \frac{R\sqrt{A}}{\sqrt{4 q J_{dark} g}} \tag{3.7}$$

Moreover, block diagram model that describes the relation between detectivity and structural parameters is implemented through VisSim as illustrated in Fig. 3.4.

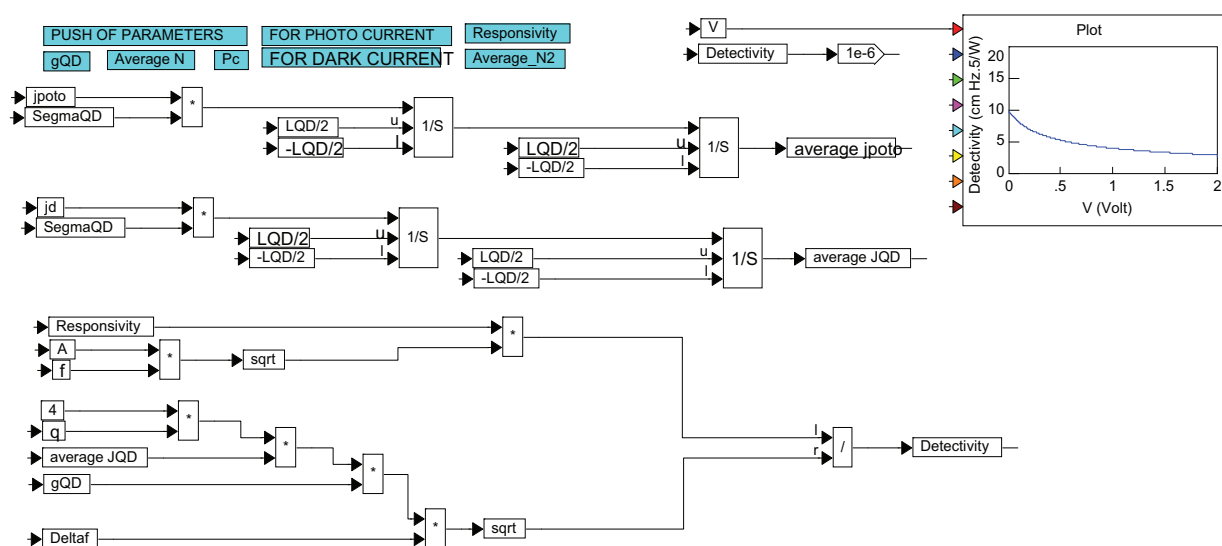


Fig. 3.4 Detectivity block diagram model of QDIPs.

## 1.5 Results and discussion

In this chapter we are interested with the calculation of different characteristics of quantum dot sources and detectors that can be used as a scintillator for the detection of gamma radiation. The values of the calculations are taken from various references as depicted in Tables 3.1-3.2 [24-31].

$n_r=3.5-5$	$\tau_0=10ps$	$L_{cav}=900\mu s$	$E_{cv}=1eV$	$\tau_{wr}=3ns$	$\tau_s=15ps$
$R_1, R_2=30\%,-90\%$	$\tau_r=2.8ns$	$A=6cm^{-1}$	$\tau_p=8.8ps$	$R=8ns$	$E_g=0.8eV$

Table 3.1 QD source parameters.



$\Sigma_{\text{QD}}=(0.1-10)\times 10^{10} \text{ cm}^{-2}$	$N_{\text{QD}}=8-10$	$T=(77-300) \text{ K}$	$\alpha =12$	$L_{\text{QD}}=(40-100) \text{ nm}$
$J_m=1.6\times 10^6 \text{ A/cm}^2$	$M=10-70$	$\rho_D=10^{10} \text{ cm}^{-3}$	$M=10-70$	$a_{\text{QD}}=(10-15) \text{ nm}$

Table 3.2 QDIP parameters.

### 1.5.1 Results of QD sources

The main target of this subsection is to study the various parameters effects on quantum dot devices for gamma radiation detection. Block diagram model using VisSim environment is used for this purpose. Consequently, the current study assists on the fact that QD devices can be used for gamma radiation detection. The effect of incident gamma radiation on the emission wavelength is deeply studied. Moreover, the effect of QD parameters on the optical gain is investigated. The modal gain is determined by calculating the amplified spontaneous emission (ASE) power. We concluded that one of the main advantages of quantum dot (QD) is their wide wavelength range. Therefore, QD sources can be used as an efficient device for gamma detection. The emission wavelength against incident gamma energy at different  $N_{\text{eff}}$  and  $V_m$  is depicted in Figs. 3.5, respectively. The wide range of emission wavelength is one of the main advantages of QD devices. However, the emission wavelength increases with the molar volume as shown in Fig. 3.5. From this study we are concluded that the emission wavelength of QD is wide. Therefore, QD can be used as an efficient device for gamma radiation detection. Furthermore, the intraband free-carrier absorption coefficient in doped semiconductors is roughly proportional to  $\lambda^2$ , which translates into larger optical waveguide losses at the longer wavelengths.

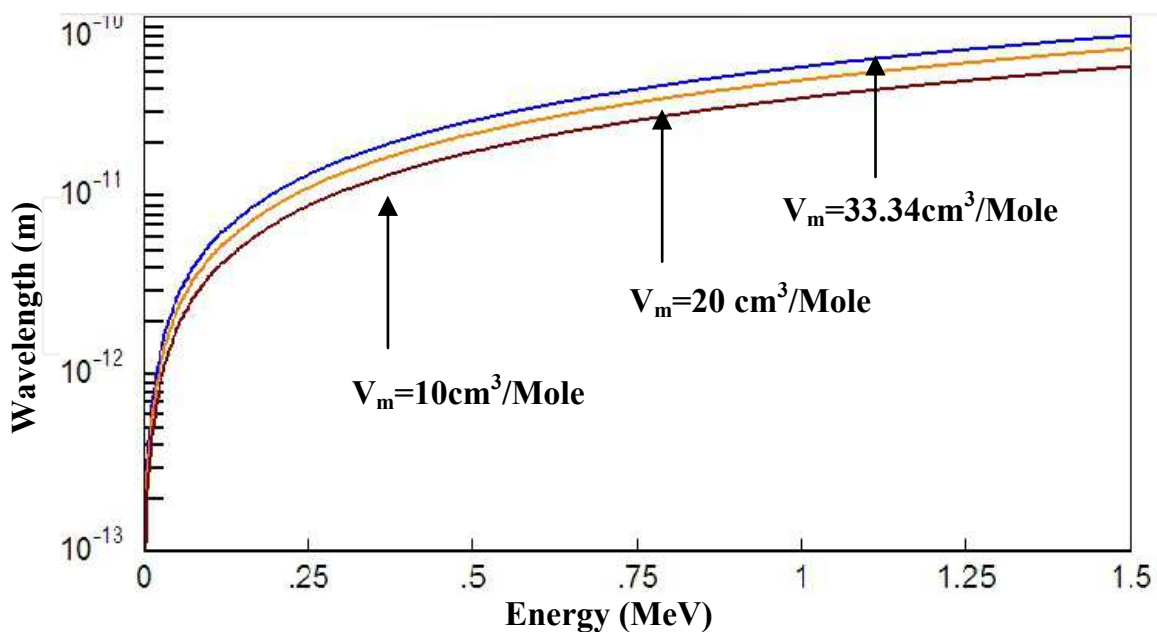


Fig. 3.5. Emission wavelength against incident gamma energy at different values of molar volume

### 1.5.2 Results of QDIPs

The change of the dark current density with the bias voltage at different sheet densities of QDs is depicted in Fig. 3.6. From this figure, the dark current increases as bias voltage increasing. The main reason for this effect is the non-optimized doping level. Moreover, high agreement between our obtained results with the published results [32] is obtained.

With an increase of  $\Sigma_{\text{QD}}$ , the dark current decreases as a result of decreasing number of electrons in quantum dots. The decrease in repulsive potential of charge carriers in quantum dots causes increase in the electron capture probability and decrease in the current gain. In the range of high QD density,  $\Sigma_{\text{QD}}$ , the dark current saturates on different levels in dependence on a bias voltage, since the number of electrons in QDs effectively decreases.

Dark current and biasing voltage results at different lateral characteristic size of quantum dot are shown in Fig 3.7. As noted from this figure, the dark current is increased with decreasing the lateral characteristic size.

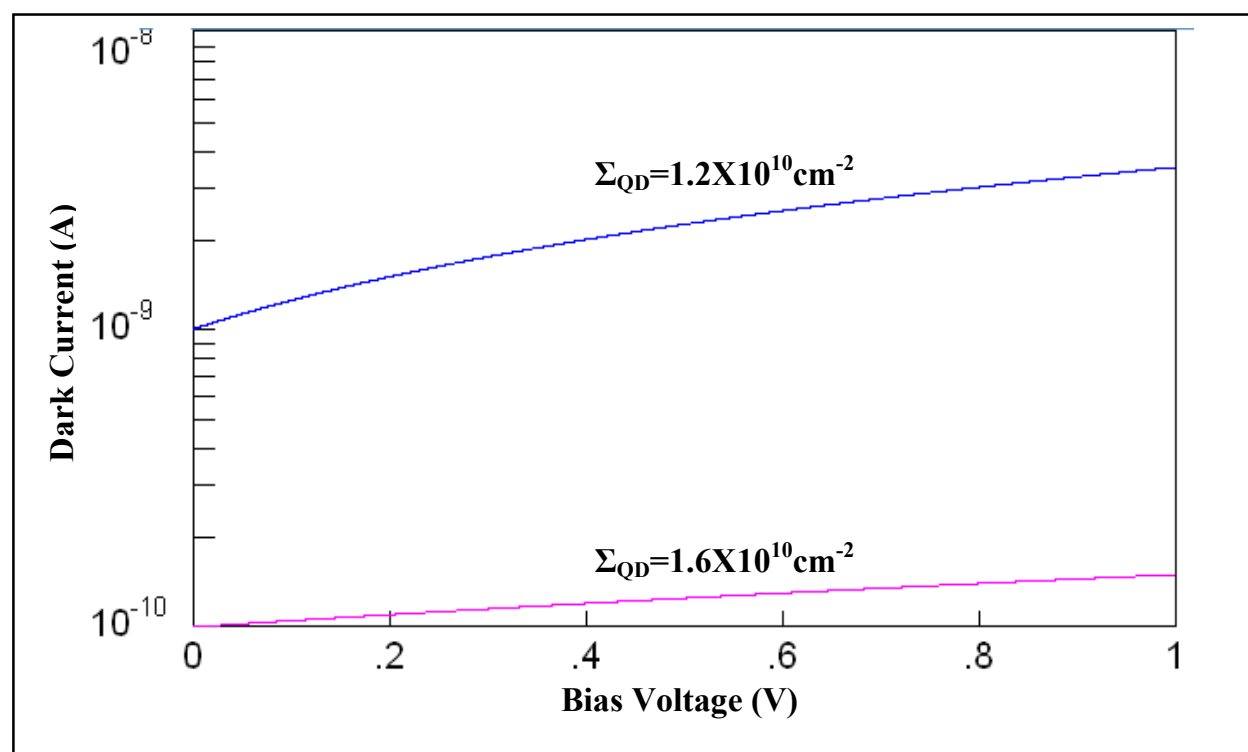


Fig. 3.6. Dark current and biasing voltage results at different quantum dot density of states.

Figures 3.8 depict the change of both dark current and photocurrent with the bias voltage. As seen in this figure, at the beginning the photocurrent is larger than the dark current because there is no thermionic emission of electron and the tunneling process of electron is so small. Then the dark current is sharply increased with the photocurrent, since more electrons are thermally emitted and losses of electrons are increased.

Figures 3.9-3.12, depicts the change of detectivity of QDIP against different parameters: temperature,  $\Sigma_{\text{QD}}$ ,  $\Sigma_{\text{D}}$ , and  $a_{\text{QD}}$ . As expected from Fig. 3.9, a rapid decrease in detectivity occurs with the increase in a temperature due to contribution of thermal generation and increasing the dark current. From Fig. 3.10, it is obvious that increasing quantum dot density

results in increasing detectivity. With increasing  $\Sigma_{\text{QD}}$ , the dark current is reduced and the unwanted noise becomes negligible. Hence detectivity is increased. As expected from Figs. 3.11-3.12, a rapid decrease of the detectivity is observed with increasing both  $\Sigma_{\text{D}}$  and the lateral sizes of QDs.

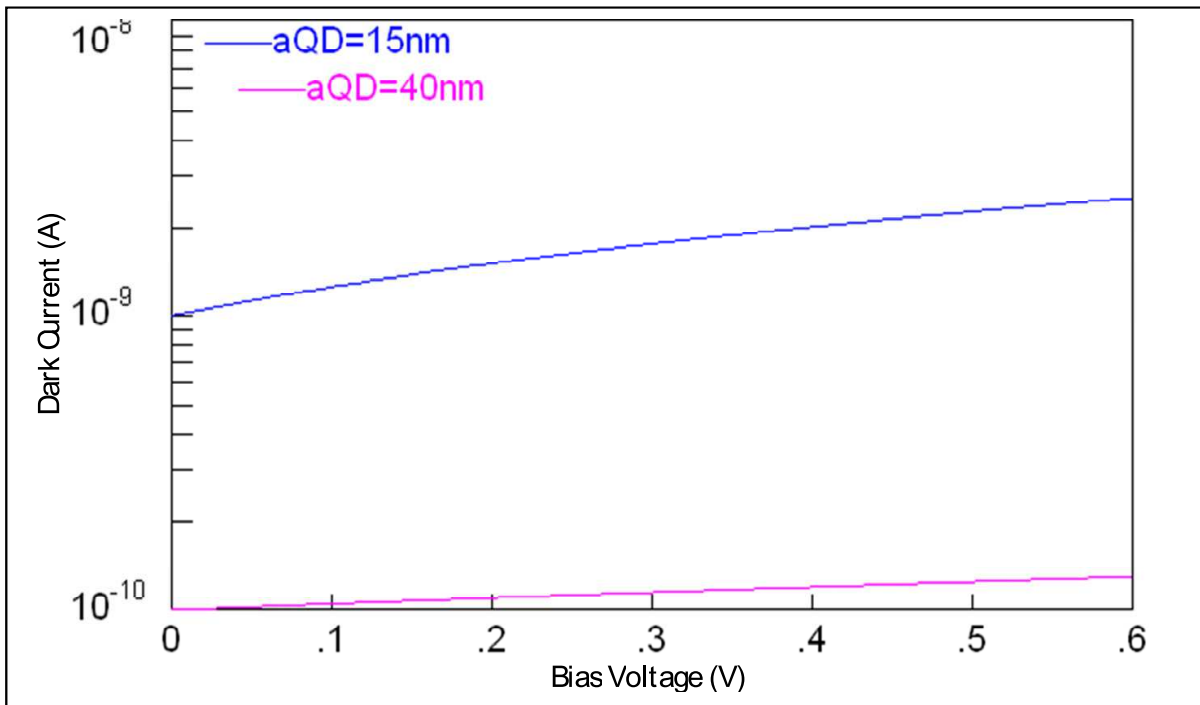


Fig. 3.7. Dark current and biasing voltage results at different lateral characteristic size of quantum dot.

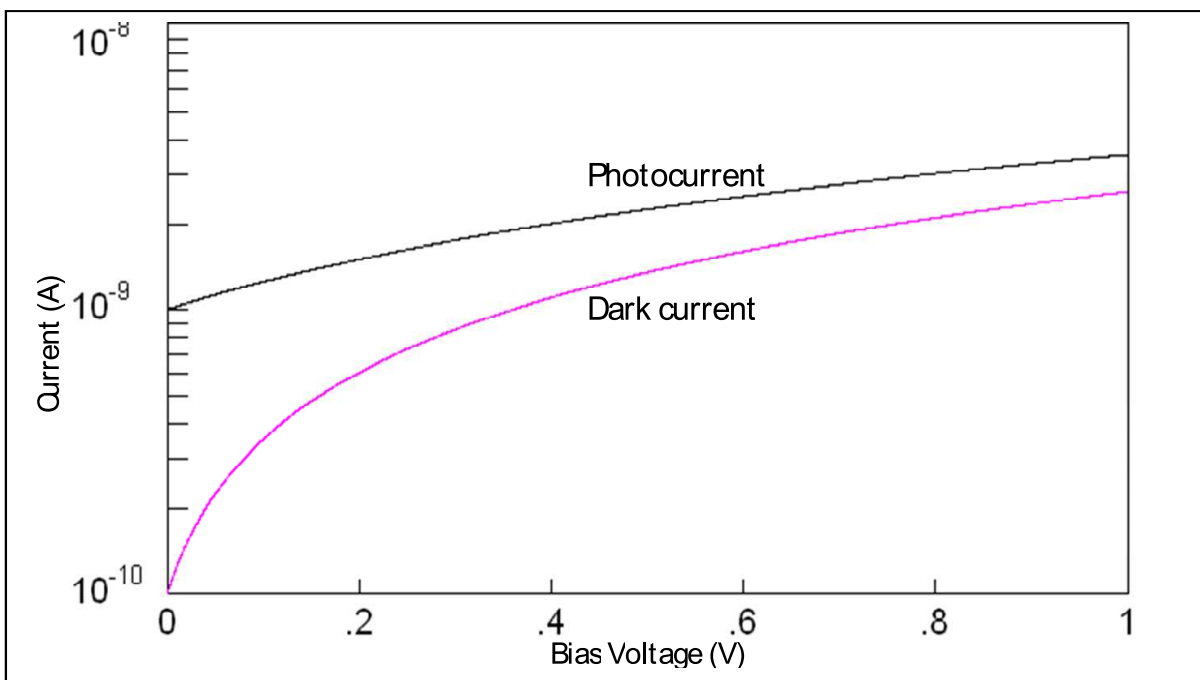


Fig. 3.8. Dark current and photocurrent as a function of the biasing voltage at different quantum dot density of states.

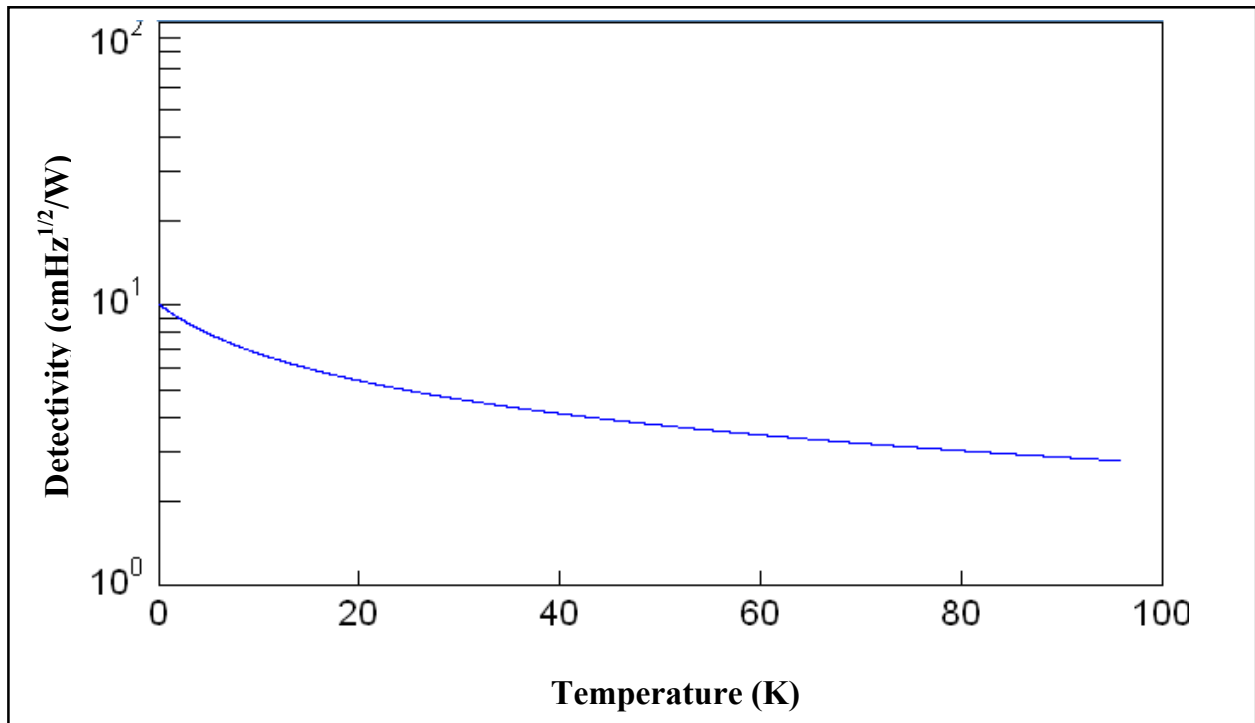


Fig. 3.9. Detectivity against temperature.

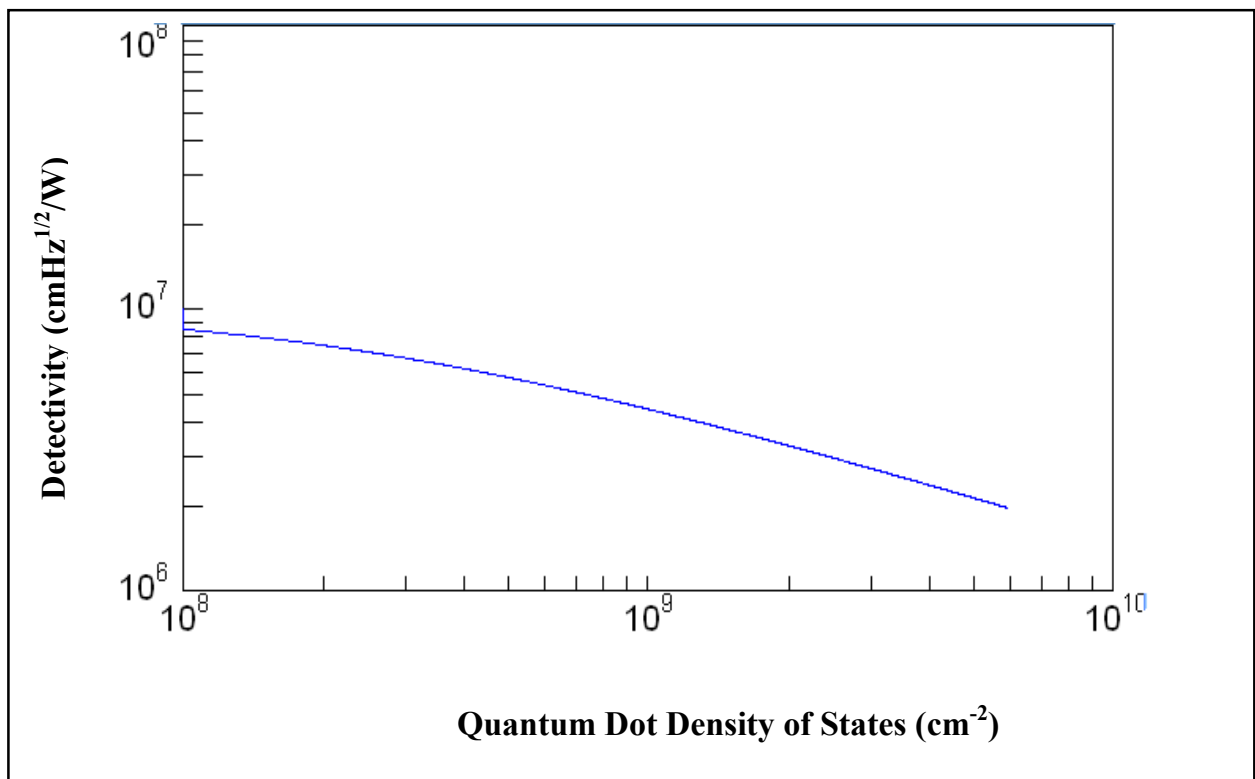
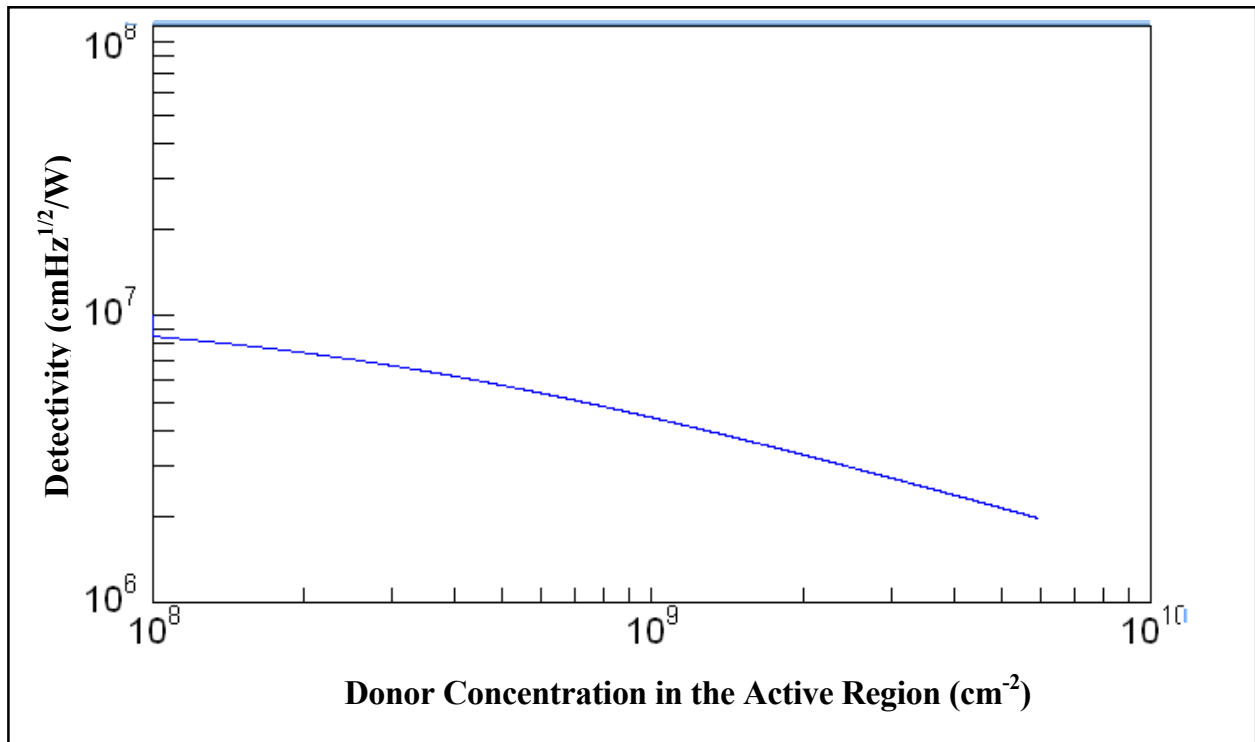
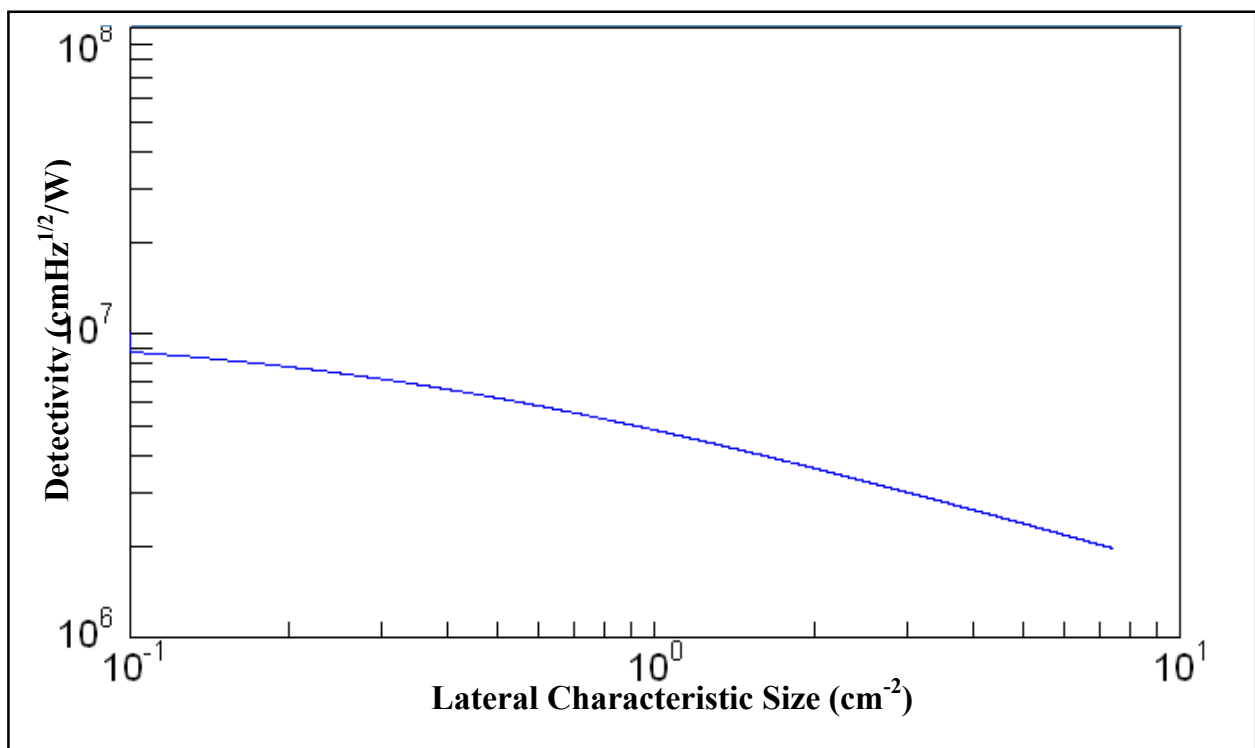


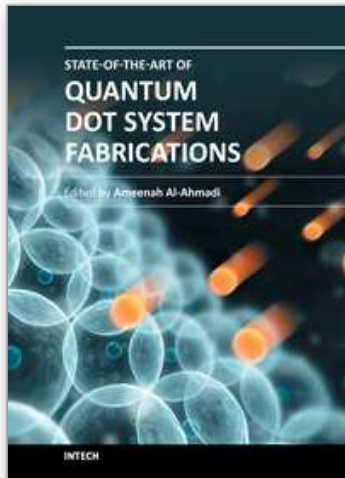
Fig. 3.10. Detectivity against quantum dot density of states.

Fig. 3.11. Detectivity against  $\Sigma_D$ .Fig. 3.12. Detectivity against  $a_{QD}$ .

## 2. References

- [1] N. J. Withers, K. Sankar, B. A. Akins, T. A. Memon, T. Gu, J. Gu, G. A. Smolyakov, M. R. Greenberg, T. J. Boyle, and M. Osiński, "Rapid degradation of CdSe/ZnS colloidal quantum dots exposed to gamma irradiation", *Applied Physics Letters*, Vol. 93, 173101, 2008.
- [2] S. E. Letant and T.-F. Wang, "Semiconductor quantum dot scintillation under  $\gamma$ -ray irradiation", *Nano Letters*, Vol. 6, No. 12, pp 2877–2880, 2006.
- [3] S. E. Letant, and T.-F. Wang, "Study of porous glass doped with quantum dots or laser dyes under alpha irradiation", *Applied Physics Letters*, Vol. 88, No. 10, pp. 103110 - 103110-3, 2006.
- [4] I. H. Campbell, B. K. Crone, "Quantum-dot/organic semiconductor composites for radiation detection", *Advanced Materials*, Vol. 18, No. 1, pp. 77-79, 2006. 63
- [5] D. S. Burgess, "Quantum dots may enable new radiation detectors", *Applied Physics Letters*, 103110, 2006.
- [6] Serge Luryi, "Impregnated semiconductor scintillator", *International Journal of High Speed Electronics and Systems*, Vol. 18, No. 4, pp. 973–982, 2008. 36
- [7] I. I. Mahmoud, and S. A. Kamel, "Using a simulation technique for switched-mode high voltage power supplies performance study", *IEEE Trans. IAS*, Vol. 34, No. 5, pp.954-952, 1998.
- [8] I. I. Mahmoud, H. A. Konber, and M. S. El\_Tokhy, "Block diagram modeling of quantum laser sources", *Optics and Laser Technology*, Vol. 42, 2010.
- [9] M. S. El\_Tokhy, "Performance improvement of optical semiconductor sources", Master thesis, Al Azhar university, 2009.
- [10] Vissim user's guide, Version 1.2, Visual solutions, Inv., West Ford, MA, 1993. 12
- [11] A. N. Immucci, A. Chamson-Reig, R. Z. Stodilka, J. J. L. Carson, K. Yu, D. Wilkinson, and C. Li, "Method for imaging quantum dots during exposure to gamma radiation", *Proc. SPIE 7925, Frontiers in Ultrafast Optics: Biomedical, Scientific, and Industrial Applications XI*, San Francisco, California, USA, 2011 [doi:10.1117/12.875379].
- [12] J. W. Mares, J. Harben, A. V. Thompson, D. W. Schoenfeld, W. V. Schoenfeld, "Gamma radiation induced degradation of operating quantum dot lasers", *IEEE Transactions on Nuclear Science*, Vol. 55, No. 2, pp. 763– 768, 2008.
- [13] V. Ryzhii, I. Khmyrova, M. Ryzhii and V. Mitin, "Comparison of dark current, responsivity and detectivity in different intersubband infrared photodetectors", *Semicond. Sci. Technol.*, Vol. 19, pp. 8–16, 2004.
- [14] Imbaby I. Mahmoud, Mohamed S. El\_Tokhy, and Hussein A. Konbe, "Model Development of Quantum Dot Devices for c Radiation Detection Using Block Diagram Programming", *Technical Brief in Nanotechnology in Engineering and Medicin Journal (NEM)*, Vol. 2, No. 3, 2011 [DOI: 10.1115/1.4004313].
- [15] Chapter 4, "Hypothesis of diffusion-limited growth", <http://scholar.lib.vt.edu/theses/available/etd-04262005-81042/unrestricted/Ch4Hypothesis.pdf>
- [16] V. Ryzhii, I. Khmyrova, V. Pipa, V. Mitin and M. Willander, "Device model for quantum dot infrared photodetectors and their dark-current characteristics", *Semiconductor Science and Technology*, Vol. 16, 331–338, 2001.

- [17] A. Nasr, "Modeling of solid state photodetectors for ionization radiation and optical fiber communications", A doctoral thesis, Al Azhar university, 2003.
- [18] Chee Hing Tan, Souye C. Liew Tat Mun, Peter Vines, John P. R. David and Mark Hopkinson, "Measurement of noise and gain in quantum dot infrared photodetectors (QDIPs)", 4th EMRS DTC Technical Conference-Edinburgh, 2007.
- [19] P. Bhattacharya, X. H. Su, S. Chakrabarti, G. Ariyawansa and A. G. U. Perera, "Characteristics of a tunneling quantum-dot infrared photodetector operating at room temperature", *Applied Physics Letters*, Vol. 86, 2005.
- [20] P. Martyniuk and A. Rogalski, "Insight into performance of quantum dot infrared photodetectors", *Bulletin of the Polish Academy Of Sciences, Technical Sciences*, Vol. 57, No. 1, 2009.
- [21] Xuejun Lu, Jarrod Vaillancourt and Mark J Meisner, "A modulation-doped longwave infrared quantum dot photodetector with high photoresponsivity", *Semicond. Sci. Technol.*, Vol. 22, pp. 993-996, 2007.
- [22] Y. Matsukura, Y. Uchiyama, H. Yamashita, H. Nishino and T. Fujii, "Responsivity-dark current relationship of quantum dot infrared photodetectors (QDIPs)", *Infrared Physics and Technology*, 2009.
- [23] Shahram Mohammad Nejad, Saeed Olyae and Maryam Pourmahyabadi, "Optimal dark current reduction in quantum well 9  $\mu\text{m}$  GaAs/AlGaAs infrared photodetectors with improved detectivity", *American Journal of Applied Sciences*, Vol. 5, No. 8, pp. 1071-1078, 2008.
- [24] D. G. Nahri, and A. N. Naeimi, "Simulation of static characteristics of self-assembled QD lasers", *World Applied Science Journal*, Vol. 11, No. 1, 2010.
- [25] V. Ryzhii, V. Pipa, I. Khmyrova, V. Mitin, and M. Willander, "Dark current in quantum dot infrared photodetectors", *Japan J. Applied Physics*, Vol. 39, No. 2000, pp. L1283-L1285, 2000.
- [26] P. Martyniuk and A. Rogalski, "Insight into performance of quantum dot infrared photodetectors", *Bulletin of the Polish Academy of Sciences, Technical Sciences*, Vol. 57, No. 1, 2009.
- [27] P. Martyniuk, S. Krishna, and A. Rogalski, "Assessment of quantum dot infrared photodetectors for high temperature Operation", *Journal of Applied Physics*, Vol. 104, 2008.
- [28] N. Li, D.-Y. Xiong, X.-F. Yang, W. Lu, W.-L. Xu, C.-L. Yang, Y. Hou, and Y. Fu, "Dark currents of GaAs/AlGaAs quantum-well infrared photodetectors", *Appl. Phys. A*, Vol. 89, pp. 701-705, 2007 [doi: 10.1007/s00339-007-4142-2].
- [29] A. Nasr, and M. B. El\_Mashade, "Theoretical comparison between quantum well and dot infrared photodetectors", *Optoelectronics IEE Proceedings*, Vol. 153, No. 4, pp. 183-190, 2006 [doi: 10.1049/ip-opt:20050029].
- [30] V. Ryzhii, I. Khmyrova, M. Ryzhii, and M. Ershov, "Comparison studies of infrared phototransistors with a quantum-well and a quantum-wire base", *Journal De Physique IV* 6, pp. C3-157-C3-161, 1996 [doi: org/10.1051/jp4:1996324].
- [31] A. Rogalski, "Insight on quantum dot infrared photodetectors", 2nd National Conference on Nanotechnology, Vol. 146, pp. 1-9, 2009.
- [32] Mohamed B. El Mashade, M. Ashry and A. Nasr, "Theoretical analysis of quantum dot infrared photodetectors", *Semiconductor Science and Technology*, Vol. 18, pp. 891-900, 2003.



## **State-of-the-Art of Quantum Dot System Fabrications**

Edited by Dr. Ameenah Al-Ahmadi

ISBN 978-953-51-0649-4

Hard cover, 172 pages

**Publisher** InTech

**Published online** 13, June, 2012

**Published in print edition** June, 2012

The book "State-of-the-art of Quantum Dot System Fabrications" contains ten chapters and devotes to some of quantum dot system fabrication methods that considered the dependence of shape, size and composition parameters on growth methods and conditions such as temperature, strain and deposition rates. This is a collaborative book sharing and providing fundamental research such as the one conducted in Physics, Chemistry, Material Science, with a base text that could serve as a reference in research by presenting up-to-date research work on the field of quantum dot systems.

### **How to reference**

In order to correctly reference this scholarly work, feel free to copy and paste the following:

Mohamed S. El-Tokhy, Imbaby I. Mahmoud and Hussein A. Konber (2012). Block Diagram Programming of Quantum Dot Sources and Infrared Photodetectors for Gamma Radiation Detection Through VisSim, State-of-the-Art of Quantum Dot System Fabrications, Dr. Ameenah Al-Ahmadi (Ed.), ISBN: 978-953-51-0649-4, InTech, Available from: <http://www.intechopen.com/books/state-of-the-art-of-quantum-dot-system-fabrications/block-diagram-programming-of-quantum-dot-sources-and-infrared-photodetectors-for-gamma-radiation>

**INTECH**  
open science | open minds

### **InTech Europe**

University Campus STeP Ri  
Slavka Krautzeka 83/A  
51000 Rijeka, Croatia  
Phone: +385 (51) 770 447  
Fax: +385 (51) 686 166  
[www.intechopen.com](http://www.intechopen.com)

### **InTech China**

Unit 405, Office Block, Hotel Equatorial Shanghai  
No.65, Yan An Road (West), Shanghai, 200040, China  
中国上海市延安西路65号上海国际贵都大饭店办公楼405单元  
Phone: +86-21-62489820  
Fax: +86-21-62489821



© 2012 The Author(s). Licensee IntechOpen. This is an open access article distributed under the terms of the [Creative Commons Attribution 3.0 License](#), which permits unrestricted use, distribution, and reproduction in any medium, provided the original work is properly cited.

IntechOpen

IntechOpen